Limited-view photoacoustic tomography utilizing backscatterers as virtual transducers

D. Wu, X. Wang, C. Tao, and X. J. Liu

Additional information on Appl. Phys. Lett.
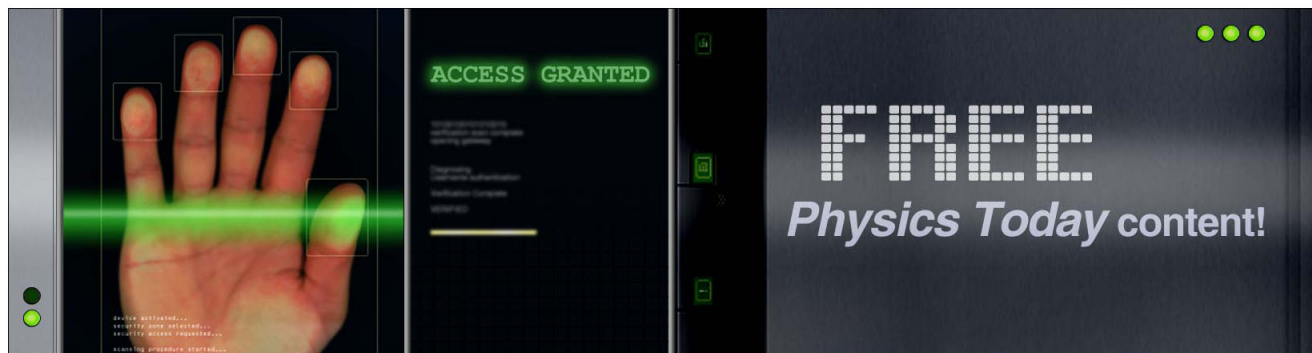
Limited-view photoacoustic tomography utilizing backscatterers as virtual transducers

D. Wu,[1] X. Wang,[2] C. Tao,[1,a)] and X. J. Liu[1,b)]

[1]Key Laboratory of Modern Acoustics, Nanjing University, Nanjing 210093, China
[2]Department of Radiology, University of Michigan, Ann Arbor, Michigan 48109, USA

In photoacoustic tomography, acoustic scattering is usually considered as a nuisance, because it distorts an incident wavefront and then induces artifacts and distortion. This work demonstrates that backscatterers could function as virtual transducers arranged behind the region of interest and are used to improve limited-view reconstruction. This idea is confirmed by both simulations and experiments. Our results suggest that enhanced photoacoustic tomography could be obtained by taking advantage of native scatterers in tissues or artificial ones injected around the region of interest. © 2011 American Institute of Physics. [doi:10.1063/1.3669512]

Photoacoustic tomography (PAT) is an emerging biomedical imaging method,[1–5] which has high image contrast and good spatial resolution in deep tissues. Moreover, the non-ionizing wave employed in PAT is much safer for biological tissues than the ionizing x-ray. Therefore, PAT has broad applications in imaging inflammation response,[6] brain function,[7] blood vessel,[8,9] etc.

Acoustic scattering is often a nuisance for PAT, since it disturbs the propagation of photoacoustic (PA) waves and degrades the image quality.[10] Facing the challenge of acoustic scattering, some efforts were made to reduce the artifacts and distortion induced by scattering.[11,12] However, scattered waves still carry the recoverable information of optical absorption. Time reversal (TR) invariance of scattering process guarantees that the information carried by scattered waves is not lost,[13] although it is perturbed. Therefore, an interesting question is naturally raised whether scattered waves could be utilized for PAT.

In this study, we propose to exploit the information carried by backscattered waves to improve limited-view PAT and develop a TR-based method to extract the information. Simulations validate the method, and experiments examine its practicability.

Let us consider the scenario in Fig. 1. Pulsed laser with an extremely short width T_p illuminates the region of interest (ROI). Tissues absorb optical energy and produce an acoustic source $q(\mathbf{r}_0,t_0) \sim A(\mathbf{r}_0)\partial H(t_0)/\partial t_0$, where $A(\mathbf{r}_0)$ and $H(t_0)$ represent the optical energy absorption deposition and the temporal profile of the laser pulse. An ultrasonic transducer array is used to record the PA pressure $p(\mathbf{r}_d,t)$ during $t \in [0,T]$, where

$$p(\mathbf{r}_d,t) = \int_0^T dt_0 \iiint_R d\mathbf{r}_0 q(\mathbf{r}_0,t_0) g(\mathbf{r}_d,t|\mathbf{r}_0,t_0). \quad (1)$$

If the dimension of strong scatterers is much larger than the PA wavelength, the Green function $g(\mathbf{r}_d,t|\mathbf{r}_0,t_0)$ can be approximated by

$$g(\mathbf{r}_d,t|\mathbf{r}_0,t_0) = g_1(\mathbf{r}_d,t|\mathbf{r}_0,t_0)$$
$$+ \iint_\Omega d\mathbf{r}_s g_2(\mathbf{r}_d,t|\mathbf{r}_0,t_0)\Theta(\theta_i,\theta_o), \quad (2)$$

where $g_1(\mathbf{r}_d,t|\mathbf{r}_0,t_0) = \delta(t-t_0-|\mathbf{r}_0-\mathbf{r}_d|/c)/4\pi|\mathbf{r}_0-\mathbf{r}_d|$, $g_2(\mathbf{r}_d,t|\mathbf{r}_0,t_0) = \delta(t-t_0-|\mathbf{r}_0-\mathbf{r}_s|/c-|\mathbf{r}_d-\mathbf{r}_s|/c)/4\pi(|\mathbf{r}_0-\mathbf{r}_s|+|\mathbf{r}_d-\mathbf{r}_s|)$, c is the speed of sound, and Ω is the boundary of scatterers. $\Theta(\theta_i,\theta_o)$ is Kronecker delta function. $\theta_i = \cos^{-1}[(\mathbf{r}_0-\mathbf{r}_s)\cdot\mathbf{n}/|\mathbf{r}_0-\mathbf{r}_s|]$ is the incident angle, $\theta_o = \cos^{-1}[(\mathbf{r}_d-\mathbf{r}_s)\cdot\mathbf{n}/|\mathbf{r}_d-\mathbf{r}_s|]$ is the reflection angle, and $\mathbf{n}$ is the outward normal vector to Ω at $\mathbf{r}_s$. The first term of the right side of Eq. (2) corresponds to direct waves (e.g., p_{d1} in Fig. 1), while the second term corresponds to backscattered wave traveling along the path given by p_{d2} and p_s in Fig. 1.

Time reversing $p(\mathbf{r}_d,t)$ to $p(\mathbf{r}_d,T-t)$ and retransmitting $p(\mathbf{r}_d,T-t)$, we have the TR field $p_{TR}(\mathbf{r}_0,t)$,

$$p_{TR}(\mathbf{r}_0,t) = \int_0^T dt_1 \iint_\Sigma d\mathbf{r}_d p(\mathbf{r}_d,T-t_1) g(\mathbf{r}_0,t|\mathbf{r}_d,t_1). \quad (3)$$

If PA signals on a whole surface enclosed ROI are detected, it can be proved $p_{TR}(\mathbf{r}_0,t) = p(\mathbf{r}_0,T-t)$.[14,15] It means $p_{TR}(\mathbf{r}_0,t)$ can precisely converge toward the source generated by optical absorption, and the eventual TR filed $p_{TR}(\mathbf{r}_0,T)$ can reveal $A(\mathbf{r}_0)$.[16] If the transducer array cannot enclose ROI, the incomplete data will degrade the image quality due to the shortage of backside information. However, when backscatterers exist, we can substitute Eq. (2) into Eq. (3) and change the integral order,

$$p_{TR}(\mathbf{r}_0,t) = \int_0^T dt_1 \left[\iint_\Sigma d\mathbf{r}_d p_t(\mathbf{r}_0,t|\mathbf{r}_d,t_1) + \iint_\Omega d\mathbf{r}_s p_s(\mathbf{r}_0,t|\mathbf{r}_s,t_1) \right], \quad (4)$$

where $p_t(\mathbf{r}_0,t|\mathbf{r}_d,t_1) = p(\mathbf{r}_d,T-t_1)g_1(\mathbf{r}_0,t|\mathbf{r}_d,t_1)$, denoting reemitting time-reversed direct waves from actual transducers, while $p_s(\mathbf{r}_0,t|\mathbf{r}_s,t_1) = \iint_\Sigma d\mathbf{r}_d p(\mathbf{r}_d,T-t_1)g_2(\mathbf{r}_0,t|\mathbf{r}_d,t_1)\Theta(\theta_i,\theta_o)$, denoting reemitting time-reversed backscattered waves. The direct waves travel along the line connecting $\mathbf{r}_d$ and $\mathbf{r}_0$, while the backscattered waves propagate along the path connecting

a)Electronic mail: taochao@nju.edu.cn.
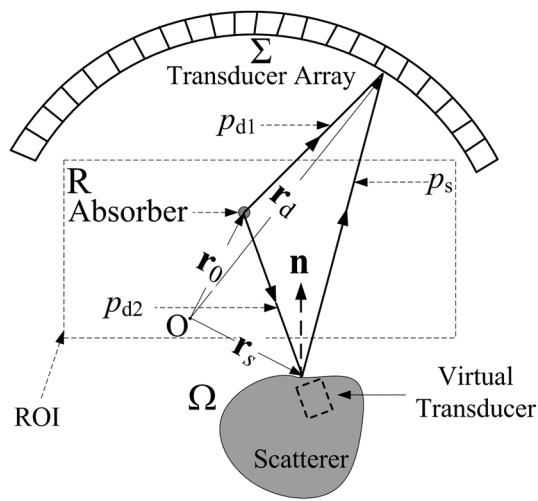b)Electronic mail: liuxiaojun@nju.edu.cn.

FIG. 1. Illustration of the principle of PAT improvement by using backscattered waves, where R is ROI, Σ represents the transducer array, and Ω is the boundary of scatterers.
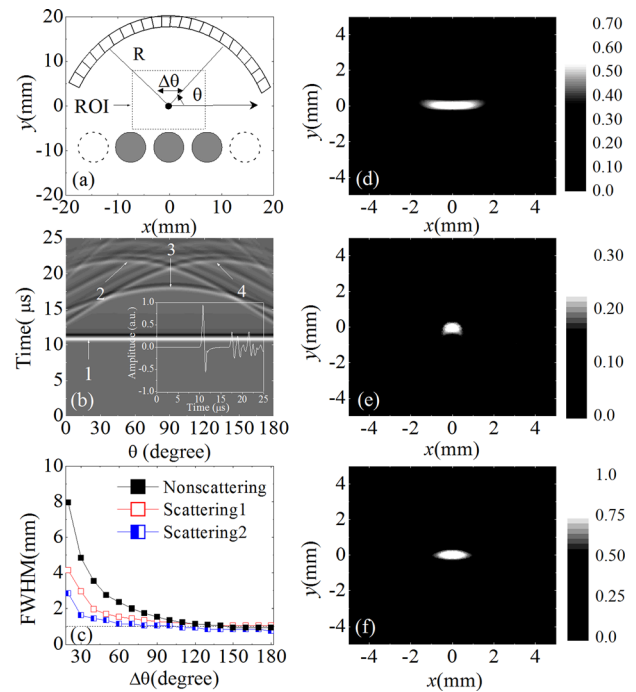

FIG. 2. (Color online) (a) Schematic illustration of numerical simulations. (b) The recorded PA field, where the wave fronts 1-4 correspond to the direct wave and three backscattered waves. The inset is the signal detected by the transducer element at $\theta = 70°$. (c) Improvement of FWHM produced by backscattered waves. The solid squares represent the results without considering backscattered signals. The empty and half-empty squares represent the scenarios with three and five scatterers, respectively. The dotted line is the actual diameter of the absorber. (d) Image obtained by using only direct waves. (e) Image obtained by using only backscattered waves. (f) Image obtained by using both direct and backscattered waves. In (d)-(f), the images are reconstructed from the data recorded by the transducer elements situated between $\theta = 70°$ and $\theta = 110°$.

absorber $\mathbf{r}_0$, boundary of scatterer $\mathbf{r}_s$ and detector $\mathbf{r}_d$. Although the back-propagating PA waves (e.g., p_{d2} in Fig. 1) cannot be directly detected by the transducer array, they could be recorded after backscattered. In this situation, scatterers [the second term in the right side of Eq. (4)] fulfill the similar function as the transducers [the first term in the right of Eq. (4)], and they are considered as virtual transducers placed at the back of ROI. Since these virtual transducers capture the back-propagating information, backscattered waves compensate for the direct waves which are not directly detected and be employed to produce better images.

In practice, the Green function involving backscattering can be measured using the acoustic method.[17,18] With the recorded $p(\mathbf{r}_d,t)$ and the known $g(\mathbf{r}_0,t|\mathbf{r}_d,t_0)$, TR field can be obtained by Eq. (3). In contrast to the previous study, where the finite element analysis is used to simulate the TR process,[16] we can reconstruct PAT images from Eq. (3).

First, numerical simulations are carried out to examine the proposed method. In Fig. 2(a), the three gray circles with 6.0 mm diameter represent scatterers. They are centered at $(-7.0\,\text{mm}, -8.0\,\text{mm})$, $(0.0\,\text{mm}, -8.0\,\text{mm})$, and $(7.0\,\text{mm}, -8.0\,\text{mm})$. The small dark circle with 1.0 mm diameter denotes an optical absorber. The acoustic parameters of the surrounding medium are $c = 1500\,\text{m/s}$ and $\rho = 1000\,\text{kg/m}^3$. PA signals are excited by Gaussian pulse laser and detected by a transducer array with 90 elements, arranged in a half-circle form with a radius 15.0 mm. The center of the half-circle is also the coordinate origin of the images. The polar angle θ indicates the position of each element of the array. $\Delta\theta$ is the aperture of the transducer array, within which the signals are used for imaging.

Four major wave fronts can be seen in the detected PA field [Fig. 2(b)]. One corresponds to direct waves, and the others correspond to scattered waves due to the three scatterers. Figures 2(d)–2(f) present the reconstructed PAT images. Fig. 2(d) is obtained from only direct waves. The absorber in the image is distorted due to incomplete data.[19,20] Scattered waves [Fig. 2(e)] also provide a clear image of the absorber, but the intensity of the image is weak because of their weak signal strength. Finally, both direct and backscattered waves

are used for imaging [Fig. 2(f)]. The obtained image gets less distortion and has high intensity.

The full width at half-maximum (FWHM) of the absorber is used to quantify the image qualities. A large aperture $(\Delta\theta > 90°)$ produces good image quality and FWHM is close to the actual diameter (1.0 mm) of the absorber.[19] A small aperture causes the deviation of FWHM from the actual value. However, if the backscattered waves are involved for imaging, the FWHM is closer to the actual value. Moreover, if two more scatterers [centered at $(-14\,\text{mm}, -8\,\text{mm})$ and $(14\,\text{mm}, -8\,\text{mm})$] are involved, the image is further improved. It is because more scatterers can form a larger-aperture virtual transducer array and capture more backside information.

Acoustic attenuation, nonlinear effect, and noise during the propagation of PA wave violate the TR invariance. These realistic factors are not considered in the simulation. It is necessary to examine our method in experiments. Fig. 3(a) presents the experimental setup. The irradiation source is a Q-switched Nd:YAG pulse laser with 532 nm wavelength, 5 ns pulse width, and 80 mJ energy. One ultrasound transducer scans around ROI along a circular orbit with 38.0 mm radius and 2° step. The detected signals are amplified (SA-230F5, NF Corporation) and recorded (PCI-5105, National Instruments) with a sampling frequency 20 MHz. Three steel rods ($c = 5700\,\text{m/s}$ and $\rho = 7980\,\text{kg/m}^3$) with 6.0 mm diameter represent scatterers, and two pencil leads with 0.5 mm
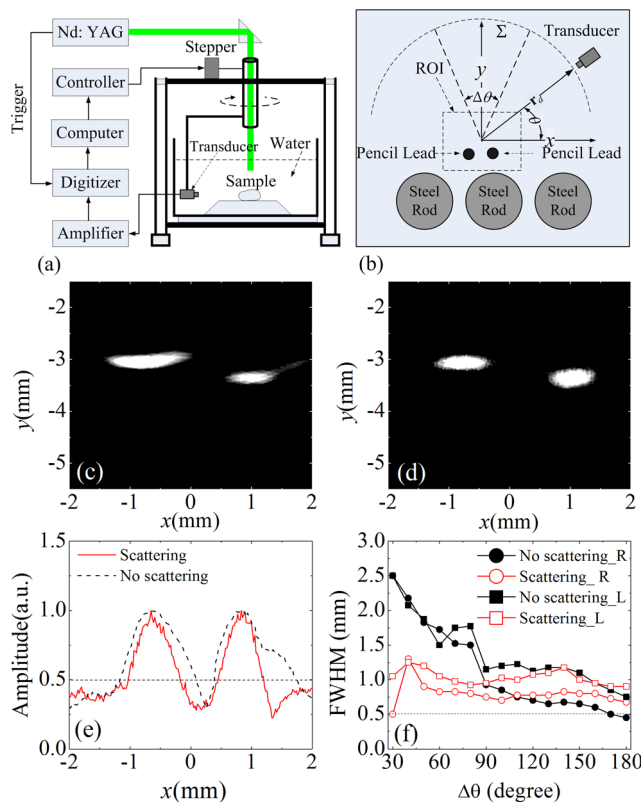
FIG. 3. (Color online) (a) Sketch map of the experimental setup. (b) A top view of the scatterers and the absorbers in the setup. (c) Image obtained without considering backscattered waves. (d) Image obtained with considering backscattered waves. (e) The profiles of intensity of the absorbers projected on the x coordinate; the dotted line is the actual diameter of the absorber. (f) Improvement of FWHM produced by backscattered waves; in the legends, R and L stand for the right and left absorbers. In (c)-(e), the data collected from $\theta = 60°$ to $120°$ are used for imaging.

diameter act as absorbers. The rods and the pencil leads are arranged parallel to each other, and perpendicular to the scanning plane. The tops of the pencil leads are on the scanning plane. Because only the tops of opaque pencils leads are radiated by light, the image of ROI is anticipated to be two circles with 0.5 mm diameter, as in Fig. 3(b).

Figures 3(c) and 3(d) present the images obtained from the signals detected from $\theta = 60°$ to $120°$. In Fig. 3(c), when only direct waves are selected for reconstruction, the image is stretched and distorted severely. However, once the backscattered waves are considered, the absorbers are less stretched and the shapes are much close to circles [Fig. 3(d)]. FWHM is determined from the profiles of maximum intensity projected on the x coordinate [Fig. 3(e)] and used to measure the improvement ascribed to the backscattered waves [Fig. 3(f)]. When the scanning angle is large, FWHM approaches to the actual diameter of the absorbers, which agrees with the conclusion of the previous study.[19] Moreover, when the scanning angle is greater than $120°$, involving backscattering wave slightly degrades the image quality. The

degradation could be explained as follows: when scanning angle is sufficiently large, the image achieved from the direct wave is good enough; in this situation, the additional virtual transducers will not improve the image significantly, but the noises brought by the backscattering degrade image. When the aperture angle is small (less than $90°$), the image reconstructed from only direct waves is seriously deformed, and the backscattered waves could significantly reduce the distortion.

In summary, it is shown that backscatterers can be considered as virtual transducers behind ROI, and the backscattered waves carry the backside information of absorbers. Therefore, the backscattered waves could be utilized to improve limited-view PAT. A method based on TR of scattered waves is proposed to recover PAT. Simulations verify the method, and experiments guarantee its practical potential. This study suggests that limited-view PAT can be improved by using native scatterers in tissues or artificial ones (e.g., injection of acoustic contrast agents or generation of a bubble wall using ultrasound vaporization of droplets) around ROI.

[1]H. Fang, K. Maslov, and L. V. Wang, Appl. Phys. Lett. **91**, 264103 (2007).
[2]B. Y. Hsieh, S. L. Chen, T. Ling, L. J. Guo, and P. C. Li, Opt. Lett. **35**, 2892 (2010).
[3]K. Kim, S. W. Huang, S. Ashkenazi, and M. O'Donnell, Appl. Phys. Lett. **90**, 223901 (2007).
[4]X. Yang, M. L. Li, and L. V. Wang, Appl. Phys. Lett. **90**, 251103 (2007).
[5]C. Kim, R. G. Qin, J. S. Xu, L. V. Wang, and R. Xu, J. Biomed. Opt. **15**, 010510 (2010).
[6]X. Wang, D. L. Chamberland, and D. A. Jamadar, Opt. Lett. **32**, 3002 (2007).
[7]X. Wang, Y. Pang, G. Ku, X. Xie, G. Stoica, and L. V. Wang, Nat. Biotechnol. **21**, 803 (2003).
[8]K. Maslov, H. F. Zhang, S. Hu, and L. V. Wang, Opt. Lett. **33**, 929 (2008).
[9]K. Jansen, A. F. W. van der Steen, H. M. M. van Beusekom, J. W. Oosterhuis, and G. van Soest, Opt. Lett. **36**, 597 (2011).
[10]X. Jin, C. H. Li, and L. V. Wang, Med. Phys. **35**, 3205 (2008).
[11]Y. Xu and L. V. Wang, IEEE Trans. Ultrason. Ferroelectr. Freq. Control. **50**, 1134 (2003).
[12]M. A. Anastasio, J. Zhang, X. C. Pan, Y. Zou, G. Ku, and L. H. V. Wang, IEEE Trans. Med. Imaging **24**, 199 (2005).
[13]E. Bossy, K. Daoudi, A. C. Boccara, M. Tanter, J. F. Aubry, G. Montaldo, and M. Fink, Appl. Phys. Lett. **89**, 184108 (2006).
[14]Y. Xu and L. V. Wang, Phys. Rev. Lett. **92**, 033902 (2004).
[15]D. Cassereau and M. Fink, IEEE Trans. Ultrason. Ferroelectr. Freq. Control. **39**, 579 (1992).
[16]D. Wu, C. Tao, and X. Liu, J. Appl. Phys. **109**, 084702 (2011).
[17]I. Vasconcelos, R. Snieder, and H. Douma, Phys. Rev. E **80**, 036605 (2009).
[18]A. Aubry and A. Derode, Phys. Rev. Lett. **102**, 084301 (2009).
[19]Y. Xu, L. V. Wang, G. Ambartsoumian, and P. Kuchment, Med. Phys. **31**, 724 (2004).
[20]C. Tao and X. Liu, Opt. Express **18**, 2760 (2010).